J. Radiat. Res., 47, 69–81 (2006)

Regular Paper

Monte Carlo Simulation of Water Radiolysis for Low-energy Charged Particles

Shuzo UEHARA[1]* and Hooshang NIKJOO[2]

Monte Carlo track structure/Water radiolysis/Time-dependent yields/LET dependence of primary yields/Electron penetration.

The paper describes the development of chemical modules simulating the prechemical and chemical stages of charged particle tracks in pure liquid water. These calculations are based on our physical track structure codes for electrons and ions (KURBUC, LEPHIST and LEAHIST) which provide the initial spatial distribution of H_2O^+, H_2O^* and subexcitation electrons at ~10^{-15} s. We considered 11 species and 26 chemical reactions. A step-by-step Monte Carlo approach was adopted for the chemical stage between 10^{-12} s and 10^{-6} s. The chemistry codes enabled to simulate the non-homogeneous chemistry that pertains to electron, proton and alpha-particle tracks of various linear energy transfers (LET). Time-dependent yields of chemical species produced by electrons and ions of different energies were calculated. The calculated primary yields (G values at 10^{-6} s) of 2.80 for OH and 2.59 for e^-_{aq} for 1 MeV electrons are in good agreement with the published values. The calculated G values at 10^{-6} s for a wide range LETs from of 0.2 to 235 keVμm^{-1} were obtained. The calculations show the LET dependence for OH and H_2O_2. The electron penetration ranges were calculated in order to discuss the role of low energy electrons.

INTRODUCTION

Monte Carlo track structure codes are important tools in radiation dosimetry and biophysical modelling and have contributed significantly to the understanding of the mechanism of radiation effects.[1–4] Among various processes in radiation-induced biological molecular effects, reactions of chemical species produced through water radiolysis are important as they contribute extensively to the yield of molecular damage. The authors have developed a suite of codes generating physical track for electrons (KURBUC - 10 eV to 10 MeV),[5] protons (LEPHIST - 1 keVu^{-1} to 1 MeVu^{-1})[6] and alpha-particles (LEAHIST - 1 keVu^{-1} to 2 MeVu^{-1})[7] in water. The ion codes provide both the track segment and the full-slowing-down modes of simulation of charged particles. The present work is an extension of these physical track structure codes describing the prechemical and chemical stages of charged particle tracks in liquid water.

The physical tracks provide the spatial distributions of the ionised and excited water molecules and subexcitation electrons at ~10^{-15} s. Subsequently, the species quickly relax during the prechemical stage which extends from 10^{-15} to ~10^{-12} s. Over this time interval, the secondary electrons become thermalized and subsequently hydrated while the ionized and excited water molecules undergo transformations which lead to the formation of radical and molecular products. Owing to the specific spatial distribution of the initial radiolytic species along the radiation tracks, the chemistry that takes place between the interval 10^{-12} and ~10^{-6} s is highly nonhomogeneous. Historically, the analytical diffusion models for the radiation chemistry of aqueous solutions have been proposed.[8,9] A Monte Carlo method is an essential tool for the simulation of this stage of nonhomogeneous chemistry. Various groups have described the track structure and radiation chemistry of water for electrons.[10–18] In these publications attention were mostly devoted to the description of energetic electron tracks for which the LET is relatively small. Sherbrooke group has also reported the development of a chemistry code for protons and electrons covering the LET range up to 20 keVμm^{-1}.[15,16]

At the heart of the development of the chemistry code lies the production of secondary electrons and the initial distributions of ionized and excited species. In this work we examine the reliability of our model and the chemical parameters used in the electron code by comparing the calculated time-dependent yields of chemical species with the available experimental and theoretical data. We present and

*Corresponding author: Phone: +81-92-642-6696,
Fax: +81-92-642-6674,
E-mail: shuzohsg@mbox.nc.kyushu-u.ac.jp
[1]School of Health Sciences, Kyushu University, Maidashi 3-1-1, Higashi-ku, Fukuoka 812-8582, Japan; [2]Center for Advanced Space Studies, USRA, NASA Johnson Space Center, Houston, Texas 77058, USA.

discuss the LET dependence of the primary yields (*G* values at 10^{-6} s) for a wide range up to 235 keVμm^{-1}.

The distribution of the distances traveled by subexcitation electrons undergoing thermalisation and recombination processes is an important critical point in the simulation of water radiolysis. Different approaches for the thermalisation distance have been proposed by many groups. In this work we have used the thermalisation distance model given by Terrissol and Beaudre.[12] This choice is examined by the penetration distances for low-energy electrons in the range between 0.1 eV and 100 keV. We also provide data on the total yields for ionization and excitation at the physical stage, and the time-dependent *G* values of chemical species for 1 keV electrons and compare with the published data.

MATERIALS AND METHODS

Physical stage

All cross sections needed for the Monte Carlo simulation of the physical stage were compiled from experimental data or use of model calculations. A comprehensive derivation of all the cross sections can be found in refs. 5 and 24 for electrons, in refs. 6 and 25 for protons and ref. 7 for alpha-particles.

The KURBUC code simulates electron tracks in water in the range 7.4 eV - 10 MeV.[5] The transport of primary and secondary electrons is explicitly followed down to 7.4 eV at which point the residual energy was deposited at a random short distance. The cross sections considered in the code were electron impact ionization and excitation, and elastic scattering. Cross section data for liquid water are scarce, as measurements are either impractical or very difficult. The only measurements to date are the 30 year old measurements of Heller in the 7-26 eV[19] using the reflection techniques and a new set of measurements by Hayashi and colleagues in the 7-160 eV[20] using the IXSS (Inelastic X-Ray Scattering Spectroscopy) method. For a review and discussion of these data see references 21 and 22. The energy loss data in liquid water can be used to construct a model of dielectric response function and in turn inelastic cross section model.[23] In the absence of a comprehensive model for liquid water cross sections, for practical reasons we use water vapor cross sections for total and partial ionization and excitation cross sections. A comprehensive review and comparison of cross section used in Monte Carlo track structure codes have been given by Uehara *et al.*[24] Inelastic cross sections for ionizations and excitations were compiled from different sources for low- and high-energy electrons. Spectra and angular distributions of the secondary electrons were obtained from experimental data and model calculations. The elastic scattering was calculated using Rutherford formula taking into account the screening parameter.

We use the term 'ions' limiting to protons H^+ and alpha-particles He^{2+}. As charged particles pass through matter, they lose energy primarily through collisions with bound electrons. Ionization cross sections for the projectile and secondary electron energies are needed to follow the history of an incident particle and its products, covering all ranges of energy transfers in individual collisions. For fast ions, the majority of energy is transferred in ionizing collisions, resulting in energetic free electrons and the potential energy of residual ions. Excitation cross sections and elastic scattering were taken into account in this work. Elastic collisions transfer little or no energy but can have a significant effect on the spatial character of the track structure at very low energies. When fast ions slow down around the Bragg peak (0.3 MeVu^{-1}), interactions involving electron capture and loss by the moving ions become an increasingly important component of the energy loss process. Charge transfer can produce residual ions without the release of free electrons, and free electrons can be ejected from the moving ion (or neutral) with no residual ions being formed. Cross section data for dressed ions H^0, He^0 and He^+ are therefore needed for a precise track simulation of low energy ions.

Table 1 shows the products after completion of the physical stage for various projectiles and energies. Excited water molecule, H_2O^*, are divided into three groups: A^1B_1, B^1A_1 and (Ry,db,de) including Rydberg states (Ry), diffuse bands (db) and dissociative excitations (de). The differences between our calculations and others such as PARTRAC code for the yields of e^-_{sub} and H_2O^+ is insignificant.[18] However, there are significant differences with the PARTRAC code in partitioning of excitations (~10%). This difference is mainly due to the differences between the set of excitation cross sections used. For protons and alpha-particles, the origin of e^-_{sub}, H_2O^+ and H_2O^* is discriminated between the ions and the secondary electrons ejected by ion impact ionization. The effect of charge transfers were calculated for low energy ions down to 3 keVu^{-1}. The electron capture and the electron loss of projectiles contribute to the large yields of H_2O^+ and e^-_{sub}, respectively. At higher ion energies the yields of e^-_{sub} and H_2O^+ formed by ionization increase due to the energetic secondary electrons. The variation of relative yields of products via H_2O^* is small over a broad range of energies and particle types.

Prechemical stage

In the prechemical stage, during the period between 10^{-15} – 10^{-12} s, the products after completion of the physical stage, e^-_{sub}, H_2O^+ and H_2O^* are converted into molecular products. Very little is known about the quantitative and qualitative production of chemical species starting from each possible excited state of liquid water molecules. Different groups use very different sets of decay probabilities. Ballarini *et al.*[18] has given a comparison table of the dissociation schemes adopted by different groups such as Toulouse,[12] London,[26] Sherbrooke,[15,16] Oak Ridge,[10,11] Tokyo,[13,17] and Milano.[18] As different codes use different set of electron inelastic scat-

Table 1. Products after completion of the physical stage (subexcitation electrons, ionised water molecules and excitations: A^1B_1, B^1A_1, Rydberg states (Ry); diffuse bands (db) and dissociative excitations (de)).

Particle		e^-_{sub}	H_2O^+	H_2O^*		
Energy				A^1B_1	B^1A_1	(Ry,db,de)
Electron						
200 eV		34.1%	29.5%	12.1%	4.6%	19.7%
1 keV		34.2	33.2	11.8	3.0	17.8
10 keV		32.7	32.6	11.6	3.9	19.2
1 MeV		33.9	33.9	11.1	3.6	17.5
Proton						
3 $keVu^{-1}$	(total)	30.9	51.2	5.2	2.2	10.5
	(ion)	30.5	50.8	2.0	1.7	8.8
	(2^{nd}-e)	0.4	0.4	3.2	0.5	1.7
10 $keVu^{-1}$	(total)	26.1	46.0	7.7	3.1	17.1
	(ion)	24.6	44.5	2.5	2.2	13.5
	(2^{nd}-e)	1.5	1.5	5.2	0.9	3.6
100 $keVu^{-1}$	(total)	31.5	31.5	11.7	4.0	21.3
	(ion)	16.8	16.8	0.6	0.7	6.8
	(2^{nd}-e)	14.7	14.7	11.1	3.3	14.5
1 $MeVu^{-1}$	(total)	32.9	32.9	10.8	3.7	19.7
	(ion)	13.6	13.6	0.4	0.5	5.3
	(2^{nd}-e)	19.3	19.3	10.4	3.2	14.4
Alpha-particle						
3 $keVu^{-1}$	(total)	40.8	43.6	6.7	1.6	7.3
	(ion)	40.0	42.8	0.9	0.8	4.1
	(2^{nd}-e)	0.8	0.8	5.8	0.8	3.2
10 $keVu^{-1}$	(total)	33.4	38.7	9.6	3.2	15.1
	(ion)	30.1	35.4	1.5	1.5	8.5
	(2^{nd}-e)	3.3	3.3	8.1	1.7	6.6
100 $keVu^{-1}$	(total)	33.6	31.2	12.3	4.0	18.9
	(ion)	15.5	13.1	0.2	0.2	2.5
	(2^{nd}-e)	18.1	18.1	12.1	3.8	16.4
1 $MeVu^{-1}$	(total)	34.2	34.1	11.1	3.5	17.1
	(ion)	11.9	11.8	0.1	0.1	1.2
	(2^{nd}-e)	22.3	22.3	11.0	3.4	15.9

tering cross sections, authors are forced to adopt different assumptions on the branching ratios in order to produce consistent *G* values for various radical species. The dissociation schemes we use in our model is similar to the one given by the Oak Ridge group for the physical products: e^-_{sub}, H_2O^+, H_2O^* consisted of A^1B_1 and (Ry,db,de). The Oak Ridge model for the B^1A_1 level use a branching ratio of 1.0 to H_2 + H_2O_2. In this work for the branching ratio we use 0.55 to H_2 + H_2O_2 and 0.45 to H_2O in order to reproduce consistent G-values for various radical species produced by electrons. Table 2 shows dissociation schemes and branching ratios for the physical products: e^-_{sub}, H_2O^+ and H_2O^*.

Table 2. Dissociation schemes and branching ratios.

Physical Product		Decay Channel	Probability (%)
e^-_{sub}		e^-_{aq}	100
H_2O^+		H_3O^+ + OH	100
H_2O^*			
	A^1B_1	H_2O	25
		H + OH	75
	B^1A_1	H_2O	45
		H_2 + H_2O_2	55
	(Ry,db,de)	H_2O	23
		H + OH	20
		H_3O^+ + OH + e^-_{aq}	57

For the spatial distribution of chemical products at the prechemical stage we assumed the same spatial distribution for the products formed by alpha-particle impact because accurate data are unavailable[15,26]. All ionized water molecules were assumed to dissociate following the H_2O^+ + H_2O → H_3O^+ + OH scheme. The displacement of H_2O^+, at the time of reaction, from its site of production is chosen from a Gaussian distribution with a mean displacement of 1.5 nm. The H_3O^+ is assumed to be at the same position as the H_2O^+ and the OH radical is positioned with random orientation at a distance of 0.29 nm.[26] In the dissociation of an excited water molecule into H and OH radicals the products are assumed to be separated by 0.87 nm on a randomly orientated line centered at the original site of H_2O^*.[26] Excitations which lead to autoionizations are treated in the same manner as ionizations. In the mechanism H_2O^* → H_2 + H_2O_2, we place one H_2O_2 species at the interaction position and H_2 is positioned at a distance of 0.36 nm.[15] The radicals and ions except e^-_{aq} were described by a Gaussian distribution with a standard deviation of 0.75 nm, as used by Schwarz[8] and Green *et al.*[27] The displacement values for all species are much smaller than the mean distance between neighboring energy deposition points in the physical stage. Therefore, the present setting does not cause a serious effect on the calculated results.

Subexcitation electrons, electrons with kinetic energy less than the first excitation potential (7.4 eV), thermalize losing their energy by successive scattering in the medium until they are in equilibrium with the surrounding molecules leading to the formation of hydrated electrons e^-_{aq}. Subexcitation electrons lose energy by rotational-vibrational interaction and are scattered by elastic interaction until they reach ther-

mal energies (~0.025 eV at room temperature). The thermalization distance which is the residual distance traveled by subexcitation electrons before becoming thermalized, depends on the initial energy of the subexcitation electrons. In the calculations the multi-step thermalization process was approximated by a single-step motion traveling the average thermalization distance with a random direction. We used the average electron thermalisation distance and its standard deviation with electron energy given by Terrissol and Beaudre.[12] The dependence of the mean thermalization distance (r in nm) on the electron subexcitation energy (E in eV) was approximated by a polynomial function of the form $r = 3.151+0.964E+1.362E^2-0.134E^3$ with an overall uncertainty of ± 50% for all r.

The recombination of subexcitation electrons with their parental ions is in competition with the thermalisation process. Upon thermalisation the electron is separated from its geminate positive ion by a distance r, although they are coulombically bound together. The probability of escape, P_{esc}, which depends on the dielectric constant of the liquid, ε, and on r is given by

$$P_{esc} = e^{-r_c/r} \quad (1)$$

where r_c is the Onsager distance defined by

$$r_c = \frac{e^2}{4\pi\varepsilon_0\varepsilon_r kT} \quad (2)$$

where e is the electronic charge, ε_0 is the dielectric constant of free space, ε_r is the relative dielectric constant of liquid water, k is the Boltzmann constant and T the temparature.[28] The value of r_c is 0.70 nm for ε_r = 80 for liquid water at 25°C. The probability of recombination of subexcitation electrons with their parent cations was ~4% of all ionization events irrespective of the particle type and its energy. In the case of geminate recombination, $e^- + H_2O^+ \rightarrow H_2O^*$, the excited water molecule is assumed to reorganize as the excited state A^1B_1.[29]

Table 3. Radical species and values of diffusion coefficients D ($10^{-9}m^2s^{-1}$).[29] The root mean square distance traveled λ (nm) was calculated according to $\lambda = (6D\tau)^{1/2}$.

Species	D	λ ($\tau = 10^{-12}$s)
OH	2.8	0.130
e^-_{aq}	4.5	0.164
H	7.0	0.205
H_3O^+	9.0	0.232
H_2	5.0	0.173
H_2O_2	2.2	0.115
HO_2	2.0	0.110
O_2	2.1	0.112
OH^-	5.0	0.173
O_2^-	2.1	0.112
HO_2^-	2.0	0.110

Chemical stage

A step-by-step approach was adopted for the chemical stage starting at 10^{-12} s to 10^{-6} s. This technique follows the diffusion of each individual species within time steps of the order of picoseconds.[11,18] During each time step of length τ, water radicals and their products were allowed to diffuse randomly with a diffusion coefficient D. Table 3 shows the

Table 4. Chemical reactions and values of reaction rate constants k (10^{10} $dm^3mol^{-1}s^{-1}$).[29] The reaction radius a (nm) is calculated by $a = k/4\pi(D_A+D_B)$.

Reaction (A + B)	Products	k	a
OH + OH	---> H_2O_2	0.6	0.1416
OH + e^-_{aq}	---> OH^-	2.5	0.4525
OH + H	---> H_2O	2.0	0.2697
OH + H_2	---> H	0.0045	0.00076
OH + H_2O_2	---> HO_2	0.0023	0.00061
OH + HO_2	---> O_2	1.0	0.2753
OH + O_2^-	---> O_2 + OH^-	0.9	0.2427
OH + HO_2^-	---> HO_2 + OH^-	0.5	0.1376
e^-_{aq} + e^-_{aq}	---> H_2 + $2OH^-$	0.55	0.0807
e^-_{aq} + H	---> H_2 + OH^-	2.5	0.2873
e^-_{aq} + H_3O^+	---> H	1.7	0.1664
e^-_{aq} + H_2O	---> OH + OH^-	1.3	0.2564
e^-_{aq} + HO_2	---> HO_2^-	2.0	0.4066
e^-_{aq} + O_2	---> O_2^-	1.9	0.3804
e^-_{aq} + O_2^-	---> OH^- + HO_2^-	1.3	0.2603
H + H	---> H_2	1.0	0.0944
H + H_2O_2	---> OH	0.01	0.00144
H + HO_2	---> H_2O_2	2.0	0.2936
H + O_2	---> HO_2	2.0	0.2904
H + OH^-	---> e^-_{aq}	0.002	0.00022
H + O_2^-	---> HO_2^-	2.0	0.2904
H_3O^+ + OH^-	---> H_2O	10.0	0.9439
H_3O^+ + O_2^-	---> HO_2	3.0	0.3571
H_3O^+ + HO_2^-	---> H_2O_2	2.0	0.2403
HO_2 + HO_2	---> H_2O_2 + O_2	0.000076	0.000025
HO_2 + O_2^-	---> O_2 + HO_2^-	0.0085	0.00274

values of diffusion coefficients for 11 species. The root mean square distance traveled, λ, was calculated according to $\lambda = (6D\tau)^{1/2}$, and the actual distance was extracted from a Gaussian distribution assuming a standard deviation of ±10%. The parameter λ distributes around 0.1 nm for $\tau = 10^{-12}$ s as shown in Table 3. At the end of each time step, the pair of species closer than their reaction radius were replaced by the reaction products. Otherwise, the species diffuse with a random direction. A reaction radius a for each pair of interacting species A and B is derived by the relationship $a = k/4\pi(D_A+D_B)$, where k is the reaction rate constant. If the distance between A and B is shorter than $2a$, the reaction occurs. In this work we considered 11 species and 26 chemical reactions. Table 4 shows chemical reactions and values of reaction rate constants k. The step-by-step technique is very time-consuming, but it allows to keep control of the spatial distribution of all species at all times, thus making it possible for direct applications to biophysical calculations of DNA damage. Our simulation codes have been used to obtain quantitative information on the formation and evolution of various transient species produced in pure water under normal condition (neutral pH, 1 atm, 25°C), using electrons, protons and alpha-particles.

RESULTS

Time dependence of yields

The reliability of the electron code has been examined by comparing with abundant experimental data. The time-dependent yields of water radicals and molecular products generated subsequent to irradiation of water with electrons were calculated in the time range between 10^{-12} s and 10^{-6} s. Figure 1 shows calculated time-dependent yields of chemical species OH, e^-_{aq}, H_2 and H_2O_2 produced by 1 MeV electron tracks (only the first 10 keV of the tracks were used for the calculations) in comparison with various published data. The initial number of species at 10^{-12} s amounts to ~1,500 per electron track, averaged over five electron tracks, for which the computing time was ~250 hours. The present calculated G values (#species/100 eV) is shown by the solid line, in comparison with the recent calculations by Ballarini *et al.*[18] (short dashed line) and Muroya *et al.*[30] (long dashed

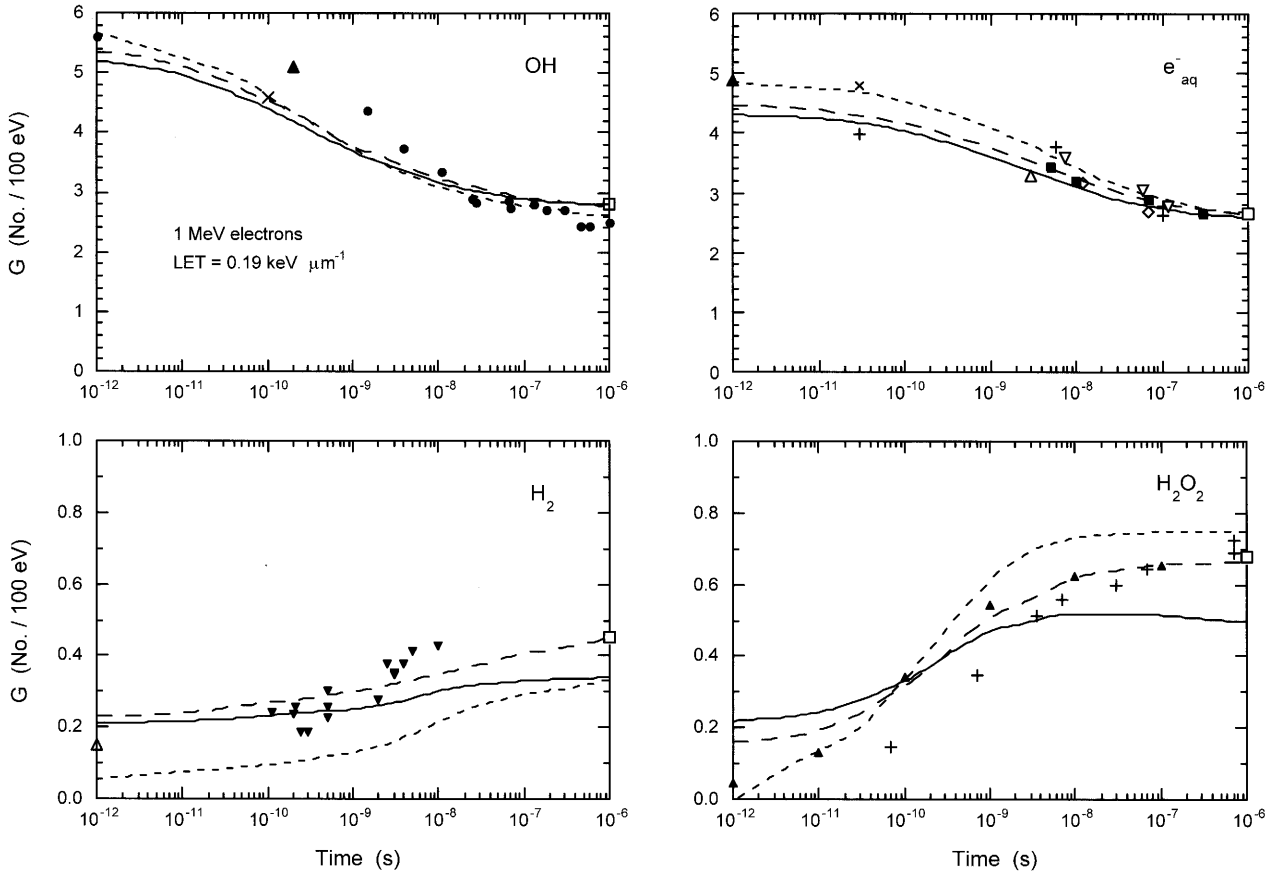

Fig. 1. Comparison of time-dependent yields of chemical species produced by 1 MeV electron tracks (the first 10 keV of the tracks only) between the present calculations and the published data. Calculations: ———— (this work);----------(ref. 18); – – – – – (ref. 30). Experiments: ● (ref. 55); x (ref. 56); ▲(ref. 35); □ (ref. 39) for OH. ▲ (ref. 14); x (ref. 57); + (ref. 58); ■ (ref. 59); ◇ (ref. 60); ▽ (ref. 61); △ (ref. 62); □ (ref. 39) for e^-_{aq}. △ (ref. 8); ▼(ref. 63); □ (ref. 39) for H_2. ▲ (ref. 14); + (ref. 55); □ (ref. 39) for H_2O_2.

line), and experimental data compiled by Muroya *et al.* (symbols).

For OH yields, the old measured values[31,32] (data not shown) stand markedly above the data in the upper left panel. Similarly we did not use the yield of e^-_{aq} measured by Jonah *et al.*[33,34] as these were recently revised downward by Bartels *et al.*[35] The standard values of the primary yields, asymptotic limit at 10^{-6} s, for fast electrons at neutral pH and 25°C (average LET = 0.3 keVμm^{-1}) are 2.80 for OH and 2.65 for e^-_{aq}.[30] The present values 2.80 and 2.59 obtained from our calculations agree well with the corresponding standard values, and the overall agreement is satisfactory.

Lower two panels in Fig. 1 present comparisons of time-dependent yields between calculations and experimental data for H_2 and H_2O_2. The present calculations for H_2O_2 does not show an enhancement in the time range greater than 10^{-8} s. The primary yields 0.50 for H_2O_2 were therefore smaller than the standard values by 30%. The initial yields (at 10^{-12} s) of four species, HO_2, O_2, O_2^- and HO_2^-, were zero and unchanged over all time. While, the variation of H_3O^+ and OH^- was similar to e^-_{aq} and H_2O_2, respectively. For all species, the present calculations are much closer to those of Muroya *et al.*[30] than those of Ballarini *et al.*[18] The calculated data of Muroya et al.[30] are in good agreement with the experimental data. Such an agreement comes about because the latter authors adjusted a number of parameters of their calculations, such as the thermalisation distance, the recombination cross section and the branching ratios used in the TRACELE[15,16], in order to fit the experimental data. On the other hand, we performed our calculations without any fitting procedures. Data shown in Fig. 1 is a good indication of new and better controlled experimental data are needed to bench mark computer codes at a higher resolution.

The water radiolysis data for electrons is essential because heavy ions loss energy by ejecting secondary electrons during slowing down. The contribution of the secondary electrons to energy deposition amounts to about 70% for the MeV region of the projectile energy. Figure 2 shows the calculated time-dependent yields of chemical species produced by 1 MeVu^{-1} protons and 1 MeVu^{-1} alpha-particles. The calculations were performed by simulating short ion track segments over which the energy loss of the initial energy of the ions is 1% (~10 keV). The values of LETs are 26.5 and 105 keVμm^{-1} for 1 MeVu^{-1} protons and 1 MeVu^{-1} alpha-particles, respectively. The experimental data of the time-dependent yields for such low energy ions are not available. However, the present calculations reproduce the experimental yields for various chemical species at 10^{-6} s where the steady state is realized.

LET and radiation type dependence of yields

Figures 1 and 2 demonstrate the time variations of the yield of radicals and molecular products depend upon the LET of the ionizing radiation. The decays of OH and e^-_{aq}

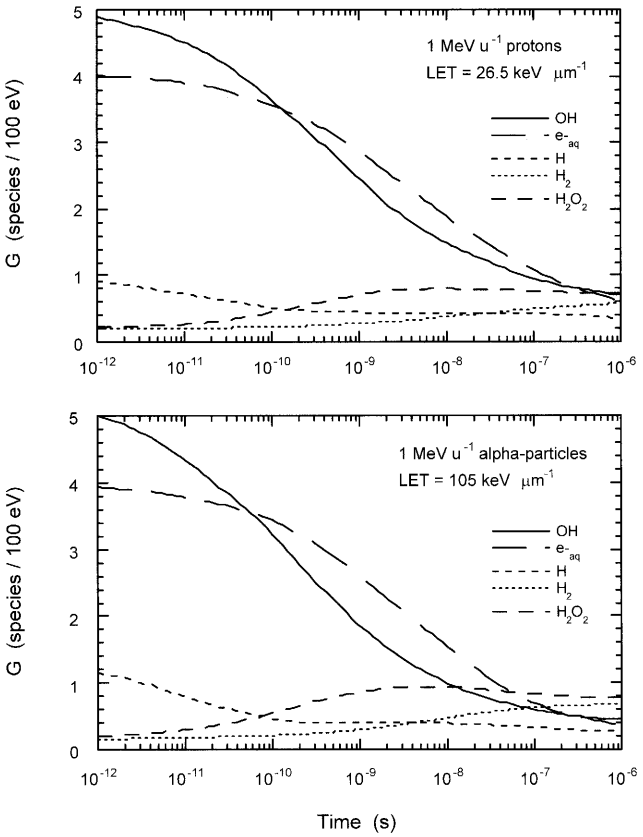

Fig. 2. Calculated time-dependent yields of chemical species produced by the first 10 keV of the tracks only for 1 MeVu^{-1} protons (upper panel) and 1 MeVu^{-1} alpha-particles (lower panel). Systematic experimental data are unavailable except at 10^{-6} s.

with 1 MeVu^{-1} protons and 1 MeVu^{-1} alpha-particles are more pronounced than those of the 1 MeV electron track. In the early development of experimental radiation chemistry it was generally believed that radiation chemical yields should be simple functions of LET, but analysis of the dependence of yields on track structure revealed a more intricate behavior. It is now known that G value is not a unique function of LET. That is, G values are different between radiations of different types even if they have the same LET, and especially for heavy ions.[36] Experimental yield of OH radicals in water by irradiation of heavy ions with various LET has been reported by Taguchi and Kojima.[37] They obtained a G value of 1.3 at about 1.5×10^{-8} s for carbon ions with LET = 105 keVμm^{-1}, while for 1 MeVu^{-1} alpha-particles with the same LET (lower panel of Fig. 2) we obtained a value of 0.9. The difference in G values at the same LET results from differences in the physical track structures of carbon ions and alpha–particles. Recently, Yamaguchi *et al.* estimated the yields of OH radicals in water irradiated by various heavy ions using the deterministic diffusion model.[38] In their model, the differential yields were represented as a function of ion energy. For 1 MeVu^{-1} protons and alpha-particles, the G_{OH}

they estimate values of 2.2 and 1.2 at 10^{-9} s and 1.1 and 0.6 at 10^{-6} s, respectively. The corresponding results from our work, as shown in Figure 2, we obtain 2.4 and 1.8 at 10^{-9} s and 0.7 and 0.4 at 10^{-6} s.

The suite of track structure codes we have developed encompass a wide range of LET for electrons, protons and alpha-particles. We performed a series of simulations in order to investigate the influence of the LET and the radiation type on the radiolytic yields. Table 5 lists the mean LET values for radiation types and energies selected for the simulations. In the table ΔE denotes the percentage of energy deposited in the first short segment of the track. The LET values were selected to be logarithmically uniform in the interval 0.2 to 235 keVμm^{-1}. The primary yields denote the yields of species remaining after, 10^{-7} s, all the spur reactions are completed give rise to various radicals.

Table 5. Mean LET for radiation types used. ΔE denotes the percentage of energy deposited in the first short segment of tracks in which LET was averaged. Total initial number of radical species produced in the segment was ~1,500 for a particle of the MeV region.

Particle	Energy		ΔE (%)	Mean LET (keVμm^{-1})	Number of history
electron	1	MeV	1	0.19	5
electron	80	keV	1	0.5	30
electron	30	keV	4	1	30
electron	12.5	keV	15	2	20
electron	3.5	keV	30	5	20
electron	2	keV	60	10	30
^{1}H	1	MeVu^{-1}	1	26.5	10
^{1}H	0.4	MeVu^{-1}	2	50	10
^{4}He	1	MeVu^{-1}	0.25	100	10
^{4}He	0.25	MeVu^{-1}	1	235	10

Figure 3 shows the variations of calculated primary yields at 10^{-6} s, for the species OH and H_2O_2 (upper panel) and e^-_{aq} and H_2 (lower panel) as a function of LET for each particle indicated by 'e', 'p' and 'α'. Lines are drawn in the LET range covered by the same particle. Smooth variation between different particles suggests that the dependence on particle type is insignificant for such light ions in the relevant LET range. The calculated values of Frongillo *et al.*[16] for protons and the measured yields of Elliot *et al.*[39] for electrons, Burns and Sims[40] for protons and alpha-particles, and Sauer *et al.*[41] for deuterons and alpha-particles are also shown for comparison. The results of our simulations for OH and H_2O_2 are in good agreement with the published data. However, the discrepancies between the present calculations and the data for e^-_{aq} and H_2 are seen at the LET range greater

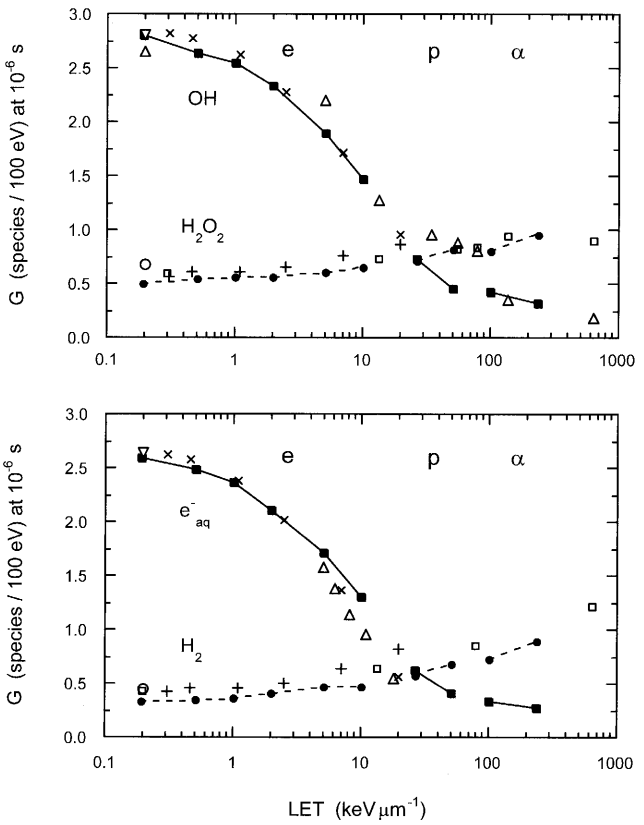

Fig. 3. Variation of the yields (G values) at 10^{-6} s for various species as a function of both LET and radiation type. LET < 10 keVμm^{-1} for electrons; 26 < LET < 50 keVμm^{-1} for protons; 100 < LET <235 keVμm^{-1} for alpha-particles. Lines are separately drawn for each radiation. Upper panel: OH and H_2O_2. Lower panel: e^-_{aq} and H_2. ■ (this work); x (ref. 16); ▽ (ref. 39); △ (ref. 40) for OH. ● (this work); + (ref. 16); ○ (ref. 39); □ (ref. 40) for H_2O_2. ■ (this work); x (ref. 16); ▽(ref. 39); △(ref. 41) for e^-_{aq}. ● (this work); + (ref. 16); (ref. 39); (ref. 40) for H_2.

than 3 keVμm^{-1}, where our data shows larger G for e^-_{aq} and smaller values for H_2. The consistency of the present simulation was confirmed by using the material balance equation, eq.(3), in which the G_H values decrease linearly from 0.55 to 0.24 with increasing LET.

$$G_{OH} + 2G_{H_2O_2} = G_{e^-_{aq}} + 2G_{H_2} G_H. \quad (3)$$

Electron penetration

The distribution of the distances traveled by subexcitation electrons undergoing thermalisation processes is an important and critical point in the simulation of water radiolysis.[42,43] In order to check the accuracy of the thermalisation distance for subexcitation electrons we used, Monte Carlo track structure calculations of electron penetration ranges were carried out at initial energies between 0.1 eV and 100 keV. The penetration distances were constructed using the code KURBUC for electron energies greater than 7.4 eV and

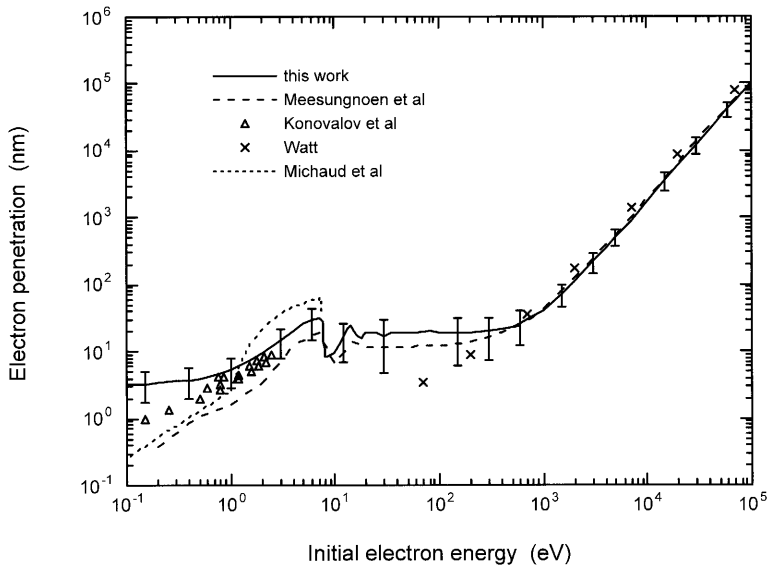

Fig. 4. Variation of the electron penetration range in water as a function of initial electron energy between 0.1 eV and 100 keV in comparison with various data. The error bars show standard deviations of our Monte Carlo simulation results. For the sake of comparison, the published penetration reported by Meesungnoen *et al.*[43] (dashed line), Konovalov *et al.*[45] (△) and Watt[44] (x), and the penetration ranges simulated for electrons between 0.1 and 7.4 eV using the amorphous ice scattering cross sections of Michaud *et al.*[46] (dotted line) are also shown. These data contain the errors as much as our value.

incorporating the single step motion of subexcitation electrons which travel the thermalisation distance with a random direction. We define the term 'penetration' as the length of the vector from the point of departure to the final position of the electron after thermalisation. It differs from the term 'range' which is customarily defined as the length of the crooked path of the electron for the complete energy degradation to thermal energy.

Figure 4 shows the present values of the electron penetration range as a function of initial electron energy in comparison with the published data. The error bars attached to this work represent standard deviations with ~ ± 50% of the corresponding penetration ranges, which arise from the variation of the average thermalisation distance. The uncertainty in our data is comparable to other model calculations. At energies greater than 300 eV, our results agree well with the Monte Carlo penetration ranges by Meesungnoen *et al.*[43] and the continuous slowing down approximation (csda) ranges reported by Watt.[44] The error bars in Meesungnoen *et al.* data[43] shows 95% confidence intervals which are comparable with our data. This result is consistent with our previous conclusion that the inverse mean free path adopted in various Monte Carlo track structure codes shows good agreement at energies higher than a few hundred eV.[21,24] In the energy region below 300 eV, our calculated electron penetration distances are greater than those of Meesungnoen *et al.*[43] Such a deviation reflects differences in the cross sections and the thermalization distance of subexcitation electrons used. The uncertainties in cross sections based on present models below 100 eV is very large amounting to more than 30–40%.[22]

The present results in the subexcitation electron energy range 0.5 and 2.5 eV show a better agreement with the experimental data having an accuracy of ± 20%,[45] while overestimating by a factor of ~3 below 0.5 eV. The dotted line for the energies below 7.4 eV was obtained by event-by-event Monte Carlo simulation using the experimental elastic and inelastic scattering cross sections of electrons in amorphous ice of Michaud *et al.*[46] The uncertainty in the measured cross sections by Sanche group is estimated as ± 25%. However, the simulation of random walk brings much greater fluctuation amounting to about ± 45% in the penetration length than the uncertainties in the cross sections themselves. The longer range implies the cross sections for ice are smaller than those for liquid water. The penetration distances for the electron energies lower than ~10 eV are directly influenced with the choice of thermalisation distance. More detailed discussions on the role of low-energy electrons will be given in the discussion section.

DISCUSSION

Cross sections for low energy electrons

Although for the spatial distributions of the ionized and excited water molecules, the sources of the ensuing chemical pathway, we use the code KURBUC, but in the absence of

a rigorous solution of energy loss in condensed phase from the 'First principle', any discussion of liquid versus vapor cross sections is accompanied with large uncertainties.[21,22,24,47] In order to discuss this issue, calculations of the G values at both the physical stage and the chemical stage were performed using the electron code KURBUC and the results are shown in comparison with the published data obtained by other Monte Carlo track structure codes.

Figure 5 shows a comparison of the calculated G values for ionization (H_2O^+) and excitation (H_2O^*) at the physical stage (~10^{-15} s) between the code KURBUC and the code OREC.[48,49] The accuracy of the G_{ion} obtained by KURBUC is verified by comparing with the experimental data (circles) of Combecher[50] along the curve for total ionization in water vapor. The values of G_{ion} and G_{exc} are almost comparable in the energy range above 1 keV, 3.2 and 3.5, respectively. The OREC code provides much larger yields 4.0 for ionization and 4.6 for excitation. Alternatively the yield ratio of ionization and excitation is expressed as 47:53 at 1 keV. Opposite results are reported by Ballarini *et al.* using PARTRAC code.[18] Although, the relative ratio of 57 : 43 is derived but the absolute values are lacking. Uehara *et al.* have compared the inverse mean free path used in various track structure codes.[24] No general agreement was seen among the codes at energies below a few hundred eV for liquid water. The differences arise mainly from the theoretical assumptions and the choice of various essential input parameters used in the codes. At present, it is difficult to set an absolute criteria for establishing benchmarks and confirming the validity of all input cross sections until a rigorous solution of the dielectric response function of the liquid water as a function of energy loss and momentum transfer has been obtained.[21,22,24]

In order to check the effect of initial numbers and spatial distributions of ionized and excited water molecules, the time-dependent yields of radical species were evaluated for the full-slowing-down tracks of 1 keV electrons. Figure 6 shows a comparison of the yields for OH (upper panel) and e^-_{aq} (lower panel) between the present work and other codes.[18,29,51] The yields at ~10^{-12} s are expected to seriously depend on the physical track structure and the prechemical model. The OH yields show differences at the early time < 10^{-9} s, although the decay characteristics for the times > 10^{-9} s are exactly the same between all calculations. The variation of e^-_{aq} yields is dispersive in comparison with OH. The dissociation scheme for ionized water molecule, $H_2O^+ + H_2O \rightarrow H_3O^+ + OH$, is common in all models. Therefore, the prechemical model on dissociation scheme and branching ratio plays an important role. Table 6 shows a comparison of electron cross sections and dissociation schemes for excited states adopted by different groups. It is difficult to conclude which is the most adequate scheme because of scarcity of experimental data. At the chemical stage the radical species diffuse by Brownian random walk and approach relatively uniform spatial distributions. Variation of the time-dependent yields at this stage decreases because various groups commonly use similar reaction schemes and chemi-

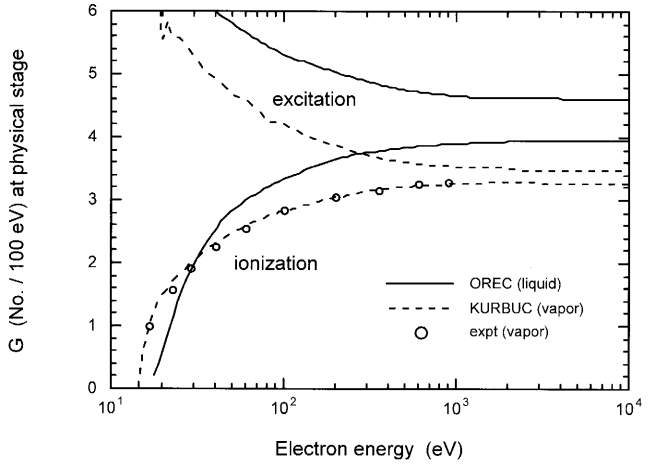

Fig. 5. Total yields for ionization and excitation as a function of initial electron energy calculated by the vapor code KURBUC in comparison with those by the liquid code OREC.[48,49] Circles along the curve for total ionization in the vapor are taken from the measured W value.[50]

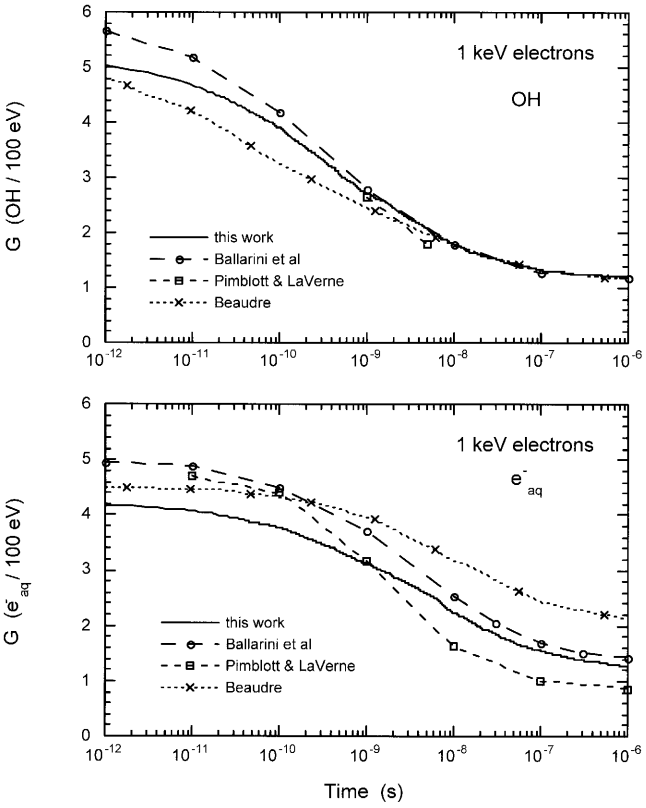

Fig. 6. Time-dependent yields of OH (upper panel) and e^-_{aq} (lower panel) following the full-slowing-down tracks of 1 keV electrons. The yields calculated by three liquid codes were taken from the literatures.[18,29,51]

Table 6. Electron cross sections and dissociation schemes for excited states adopted by different groups.

	this work	ref. 18	ref. 29	ref. 51
electron cross sections	vapor	liquid	liquid	liquid
H_2O^*				
H + OH				75%
H_2 + O				25%
H_2O^* (A^1B_1)				
H_2O	25%	35%	–	
H + OH	75%	65%	100%	
H_2O^* (B^1A_1)				
H_2O	45%	23%	–	
H_3O^+ + OH + e^-_{aq}	–	50%	–	
H + OH	–	20%	–	
2H + O	–	3.9%	–	
H_2 + O	–	–	100%	
H_2 + H_2O_2	55%	3.2%	–	
H_2O^* (Ry,db,de)				
H_2O	23%	50%	–	
H + OH	20%	–	–	
H_3O^+ + OH + e^-_{aq}	57%	50%	100%	

cal parameters. The major factor which dominates the simulation of water radiolysis is therefore calculation models and parameters adopted in prechemical and chemical processes, rather than the generator of the physical track.

Role of low-energy electrons

At low electron energies a quantitative description of electron transport in liquid water is still a challenging problem, due mainly to the scarcity of reliable scattering cross section data. Ballarini *et al.*[18] have approximated the mean thermalisation distance $<r_{therm}>$ on the electron subexcitation energy E by a straight line, $<r_{therm}> = 1.8E$ based on the model proposed by Ritchie *et al.*[52] The thermalisation distance of Meesungnoen *et al.* [43] has been obtained by event-by-event basis from the initial energies of subexcitation electrons until they get thermalized. The elastic and inelastic scattering cross sections used for the subexcitation electrons were based on the data of Michaud and Sanche obtained from slow (1-18 eV) electron-impact experiments on thin amorphous ice film condensed at 14 K.[53,54] However, Meesungnoen and colleagues increased these by an arbitrary factor of 2 to account for the differences between solid- and liquid-phase cross sections. Cobut *et al.* also have stated that solid cross sections had to be increased by a factor of two in order to reproduce the observed time dependence of the yield of hydrated electrons (e^-_{aq}).[15]

Figure 7 shows the average thermalisation distance of subexcitation electrons as a function of electron energy.

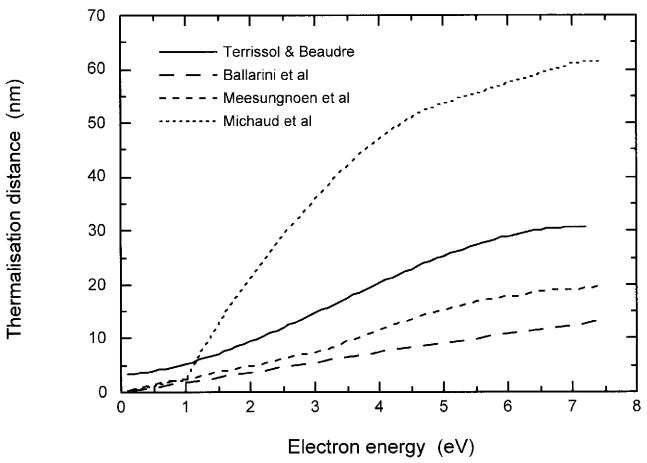

Fig. 7. Variation of the thermalisation distance of subexcitation electrons in water as a function of initial electron energy < 7.4 eV. The solid line represents the thermalisation distance of Terrissol and Beaudre[12] which is used for the present work. The long dashed line (Ballarini *et al.*[18]) and the short dashed line (Meesungnoen *et al.*[43]) are taken from the literatures. Dotted line was obtained by Monte Carlo simulations using the experimental scattering cross sections of electrons in amorphous ice of Michaud *et al.*[46] Standard deviations of all data are estimated ~ ± 45%.

Standard deviations of all data are estimated to be ~ ± 50% of the corresponding distance at all energies. The thermalisation distances used by Ballarini *et al.*[18] and Meesungnoen *et al.*[43] are shorter than our data. We estimated the thermalisation distances using the newly reported amorphous ice cross section data of Michaud *et al.*[46] The latter authors provide new data for electron energies up to 100 eV but those in the subexcitation energy range are almost the same as the previous reports.[53,54] Although Michaud and Sanche did not present thermalisation distances explicitly, we calculated the thermalisation distances of their data by Monte Carlo simulation method using their published cross sections. In our work we did not multiply the solid cross sections by a factor 2, therefore the calculated distances show more than twice enhancement in comparison with other data for the liquid phase. If the factor 2 was taken into account, the thermalization distances will be reduced by a half and approaches the data of Terrissol and Beaudre.

The effect of thermalisation distance on the time-dependent yield was investigated by adopting the shorter thermalisation distances of Ballarini *et al.* and the longer ones of Michaud *et al.* In both cases, the calculated yield of OH radicals shows similarity to the data of Terrissoll and Beaudre. The shorter thermalisation distance data provide a faster decay yields for e^-_{aq} as a function of time in contrary to the longer thermalisation distances. This result is reasonable because spatial distributions of e^-_{aq} (hydrated electrons) formed at the end of the track of e^-_{sub} (subexcitation electrons) widely extends. It is concluded that the choice of thermalisation model in this work is appropriate if keeping the

other parameters of the prechemical and chemical stage unchanged.

CONCLUSIONS

In this paper we described the development of a new chemistry code which simulates the prechemical and chemical stages of ionising radiations in liquid water. The code is based on our database for the simulation of tracks of electrons and ions. A step-by-step Monte Carlo method was adopted for the chemical stage. Simulation of such events consumes large cpu's and amounts to several hundred hours for 1 MeV electrons. Our simulation codes were used to obtain quantitative information on the formation and evolution of various transient species produced in pure neutral water under normal conditions for electrons, protons and alpha-particles. The yields of radiolytic species, such as OH, e^-_{aq}, H, H_2 and H_2O_2, were calculated from 10^{-12} to 10^{-6} s. The time dependent yields for the species for 1 MeV electron tracks (only the first 10 keV was used) were compared with the recently compiled theoretical and experimental data. LET effects on the primary yields at 10^{-6} s were studied using short segments of charged particle tracks in the range 0.2 – 235 keVμm^{-1}. The present calculations for OH and H_2O_2 agreed with experimental data for a wide range of LET. On the other hand our simulations provided greater primary yields for e^-_{aq} compared to the published data by ~10%. The electron penetration ranges were evaluated to test the effect of various thermalisation distance for subexcitation electrons. Finally, it is concluded that the dominant factor which influences the simulation of water radiolysis is the treatment of prechemical and chemical stages, not necessarily in the physical track structure. The present chemistry code enables us to investigate the radiation-induced biological and molecular effects in radiation chemistry and biology.

REFERENCES

1. Paretzke H. G. (1987) Radiation track structure theory, In Kinetics of Non-homogeneous Processes (G. R. Freeman, Ed.) Wiley, New York, pp 89–170.
2. Mozumder, A. and Hatano, Y. (2004) Charged particle and photon interactions with matter: chemical, physicochemical, and biological consequences with applications. Marcel Dekker, New York.
3. Nikjoo, H. and Uehara, S. (2004) Track structure studies of biological systems. In: Mozumder, A. and Hatano, Y. (eds) Charged particle and photon interactions with matter: chemical, physicochemical, and biological consequences with applications. pp. 491–531, Marcel Dekker, New York.
4. Nikjoo, H., Goorley, T., Fulford, J., Takakura, K. and Ito, T. (2002) Quantitative analysis of the energetics of DNA damage. Radiat. Prot. Dosim. **99**: 91–98.
5. Uehara, S., Nikjoo, H. and Goodhead, D. T. (1993) Cross sections for water vapour for the Monte Carlo electron track structure code from 10 eV to the MeV region. Phys. Med. Biol. **38**: 1841–1858.
6. Uehara, S., Toburen, L. H. and Nikjoo, H. (2001) Development of a Monte Carlo track structure code for low-energy protons in water. Int. J. Radiat. Biol. **77**: 139–154.
7. Uehara, S. and Nikjoo, H. (2002) Monte Carlo track structure code for low-energy alpha-particles in water. J. Phys. Chem. **B 106**: 11051–11063.
8. Schwarz, H. A. (1969) Applications of the spur diffusion model to the radiation chemistry of aqueous solutions. J. Phys. Chem. **73**: 1928–1937.
9. Noyes, R. M. (1961) Effects of diffusion rates on chemical kinetics. In: Porter, G. and Stevens, B. (eds) Progress in reaction kinetics. Vol. 1., pp. 129–160, Pergamon, Oxford.
10. Turner, J. E., Hamm, R. N., Wright, H. A., Ritchie, R. H., Magee, J. L., Chatterjee, A. and Bolch, W. E. (1988) Studies to link the basic radiation physics and chemistry of liquid water. Radiat. Phys. Chem. **32**: 503–510.
11. Hamm, R. N., Turner, J. E. and Stabin, M. G. (1998) Monte Carlo simulation of diffusion and reaction in water radiolysis - a study of reactant 'jump through' and jump distances. Radiat. Environ. Biophys. **36**: 229–234.
12. Terrissol, M. and Beaudre, A. (1990) Simulation of space and time evolution of radiolytic species induced by electrons in water. Radiat. Prot. Dosim. **31**: 175–177.
13. Tomita, H., Kai, M., Kusama, T. and Ito, A. (1997) Monte Carlo simulation of physicochemical processes of liquid water radiolysis. Radiat. Environ. Biophys. **36**: 105–116.
14. Pimblott, S. M. and LaVerne, J. A. (1997) Stochastic simulation of the electron radiolysis of water and aqueous solutions. J. Phys. Chem. **A 101**: 5828–5838.
15. Cobut, V., Frongillo, Y., Patau, J. P., Goulet, T., Fraser, M. J. and Jay-Gerin, J. P. (1998) Monte Carlo simulation of fast electron and proton tracks in liquid water - I. Physical and physico-chemical aspects. Radiat. Phys. Chem. **51**: 229–243.
16. Frongillo, Y., Goulet, T., Fraser, M. J., Cobut, V., Patau, J. P. and Jay-Gerin, J. P. (1998) Monte Carlo simulation of fast electron and proton tracks in liquid water - II. Nonhomogeneous chemistry. Radiat. Phys. Chem. **51**: 245–254.
17. Watanabe, R. and Saito, K. (2001) Monte Carlo simulation of water radiolysis in oxygenated condition for monoenergetic electrons from 100 eV to 1 MeV. Radiat. Phys. Chem. **62**: 217–228.
18. Ballarini, F., Biaggi, M., Merzagora, M., Ottolenghi, A., Dingfelder, M., Friedland, W., Jacob, P. and Paretzke, H. G. (2000) Stochastic aspects and uncertainties in the prechemical and chemical stages of electron tracks in liquid water: a quantitative analysis based on Monte Carlo simulations. Radiat. Environ. Biophys. **39**: 179–188.
19. Heller, J. M., Hamm, R. N., Birkhoff, R. D. and Painter, L. R. (1974) Collective oscillation in liquid water. J. Chem. Phys. **60**: 3483–3486.
20. Hayashi, H., Watanabe, N., Udagawa, Y. and Kao, C. C. (2000) The complete optical spectrum of liquid water measured by inelastic x-ray scattering. Proc. Natl. Acad. Sci. **97**: 6264–6266.
21. Emfietzoglou, D. and Nikjoo, H. (2005) The effect of model

approximations on single-collision distributions of low-energy electrons in liquid water. Radiat. Res. **163**: 98–111.
22. Emfietzoglou, D, Cucinotta, F. A. and Nikjoo, H. (2005) A complete dielectric response model for liquid water: A solution of the Bethe ridge problem. Radiat. Res. **164**: 202–211.
23. Dingfelder, M., Hantke, D., Inokuti, M. and Paretzke, H. G. (1998) Electron inelastic-scattering cross sections in liquid water. Radiat. Phys. Chem. **53**: 1–18.
24. Uehara, S., Nikjoo, H. and Goodhead, D. T. (1999) Comparison and assessment of electron cross sections for Monte Carlo track structure codes. Radiat. Res. **152**: 202–213.
25. Uehara, S., Toburen, L. H., Wilson, W. E., Goodhead, D. T. and Nikjoo, H. (2000) Calculations of electronic stopping cross sections for low-energy protons in water. Radiat. Phys. Chem. **59**: 1–11.
26. Hill, M. A. and Smith, F. A. (1994) Calculation of initial and primary yields in the radiolysis of water. Radiat. Phys. Chem. **43**: 265–280.
27. Green, N. J. B., Pilling, M. J., Pimblott, S. M. and Clifford, P. (1990) Stochastic modelling of fast kinetics in a radiation track. J. Phys. Chem. **94**: 251–258.
28. Freeman, G. R. (1987) Ionization and charge separation in irradiated materials. In: Freeman, G. R. (ed.) Kinetics of nonhomogeneous processes. pp. 19–87, Wiley, New York.
29. Beaudre, A. (1988) These de l'Universite Paul Sabatier, Toulouse, France, no. 371.
30. Muroya, Y., Meesungnoen, J., Jay-Gerin, J. P., Filali-Mouhim, A., Goulet, T., Katsumura, Y. and Mankhetkorn, S. (2002) Radiolysis of liquid water: An attempt to reconcile Monte-Carlo calculations with new experimental hydrated electron yield data at early times. Can. J. Chem. **80**: 1367–1374.
31. Jonah, C. D. and Miller, J. R. (1977) Yield and decay of the OH radical from 200 ps to 3 ns. J. Phys. Chem. **81**: 1974–1976.
32. Chernovitz, A. C. and Jonah, C. D. (1988) Isotopic dependence of recombination kinetics in water. J. Phys. Chem. **92**: 5946–5950.
33. Jonah, C. D., Hart, E. J. and Matheson, M. S. (1973) Yields and decay of the hydrated electron at times greater than 200 picoseconds. J. Phys. Chem. **77**: 1838–1843.
34. Jonah, C. D., Matheson, M. S., Miller, J. R. and Hart, E. J. (1976) Yield and decay of the hydrated electron from 100 ps to 3 ns. J. Phys. Chem. **80**: 1267–1270.
35. Bartels, D. M., Cook, A. R., Mudaliar, M. and Jonah, C. D. (2000) Spur decay of the solvated electron in picosecond radiolysis measured with time-correlated absorption spectroscopy. J. Phys. Chem. **A 104**: 1686–1691.
36. Magee, J. L. and Chatterjee, A. (1987) Track reactions of radiation chemistry. In: Freeman, G. R. (ed.) Kinetics of nonhomogeneous processes. pp. 171–214, Wiley, New York.
37. Taguchi, M. and Kojima, T. (2005) Yield of OH radicals in water under high-density energy deposition by heavy-ion irradiation. Radiat. Res. **163**: 455–461.
38. Yamaguchi, H., Uchihori, Y., Yasuda, N., Takada, M. and Kitamura, H. (2005) Estimation of yields of OH radicals in water irradiated by ionizing radiation. J. Radiat. Res. **46**: 333–341.
39. Elliot, A. J., Chenier, M. P. and Ouellette, D. C. (1993) Temperature dependence of g values for H_2O and D_2O irradiated with low linear energy transfer radiation. J. Chem. Soc. Faraday Trans. **89**: 1193–1197.
40. Burns, W. G. and Sims, H. E. (1981) Effect of radiation type in water radiolysis. J. Chem. Soc. Faraday Trans. 1, **77**: 2803–2813.
41. Sauer, Jr, M. C., Schmidt, K. H., Hart, E. J., Naleway, C. A. . and Jonah, C. D. (1977) LET dependence of transient yields in the pulse radiolysis of aqueous systems with deuterons and alpha particles. Radiat. Res. **70**: 91–106.
42. Goulet, T., Patau, J. P. and Jay-Gerin, J. P. (1990) Thermalisation and recombination of subexcitation electrons in solid water. Radiat. Prot. Dosim. **31**: 33–36.
43. Meesungnoen, J., Jay-Gerin, J. P., Filali-Mouhim, A. and Mankhetkorn, S. (2002) Low-energy electron penetration range in liquid water. Radiat. Res. **158**: 657–660.
44. Watt, D. E. (1996) Quantities for Dosimetry of Ionizing Radiations in Liquid Water. Taylor & Francis, London.
45. Konovalov, V. V., Raitsimring, A. M. and Tsvetkov, Yu. D. (1988) Thermalization lengths of "subexcitation electrons" in water determined by photoinjection from metals into electrolyte solutions. Radiat. Phys. Chem. **32**: 623–632.
46. Michaud, M., Wen, A. and Sanche, L. (2003) Cross sections for low-energy (1-100 eV) electron elastic and inelastic scattering in amorphous ice. Radiat. Res. **159**: 3–22.
47. Nikjoo, H., Terrissol, M., Hamm, R. N., Turner, J. E., Uehara, S., Paretzke, H. G. and Goodhead, D. T. (1994) Comparison of energy deposition in small cylindrical volumes by electrons generated by Monte Carlo track structure codes for gaseous and liquid water. Radiat. Prot. Dosim. **52**: 165–169.
48. Hamm, R. N., Turner, J. E., Ritchie, R. H. and Wright, H. A. (1985) Calculation of heavy-ion tracks in liquid water. Radiat. Res. **104** (Suppl.): S20–S26.
49. Paretzke, H. G., Turner, J. E., Hamm, R. N., Wright, H. A. and Ritchie, R. H. (1986) Calculated yields and fluctuations for electron degradation in liquid water and water vapour. J. Chem. Phys. **84**: 3182–3187.
50. Combecher, D. (1980) Measurements of W values of low-energy electrons in several gases. Radiat. Res. **84**: 189–218.
51. Pimblott, S. M. and LaVerne, J. A. (1998) Effect of electron energy on the radiation chemistry of liquid water. Radiat. Res. **150**: 159–169.
52. Ritchie, R. H., Hamm, R. N., Turner, J. E. and Bolch, W. E. (1994) Interaction of low-energy electrons with condensed matter: relevance for track structure. In: Varma, N. and Chatterjee, A. (eds) Computational approaches in molecular radiation biology. pp. 155–166, Plenum, New York.
53. Michaud, M. and Sanche, L. (1987a) Total cross section for slow-electrons (1-20 eV) scattering in solid H_2O. Phys. Rev. **A 36**: 4672–4683.
54. Michaud, M. and Sanche, L. (1987b) Absolute vibrational excitation cross sections for slow-electron (1-18 eV) scattering in solid H_2O. Phys. Rev. **A 36**: 4684–4699.
55. LaVerne, J. A. (2000) OH radicals and oxidizing products in the gamma radiolysis of water. Radiat. Res. **153**: 196–200.
56. Jay-Gerin, J. P. and Ferradini, C. (2000) A new estimate of the OH radical yield at early times in the radiolysis of liquid

water. Chem. Phys. Lett. **317**: 388–391.
57. Sumiyoshi, T. and Katayama, M. (1982) The yield of hydrated electron at 30 picoseconds. Chem. Lett. **12**: 1887–1890.
58. Wolff, R. K., Bronskill, M. J., Aldrich, J. E. and Hunt, J. W. (1973) Picosecond pulse radiolysis. IV. Yield of the solvated electron at 30 picoseconds. J. Phys. Chem. **77**: 1350–1355.
59. Shiraishi, H., Katsumura, Y., Hiroishi, D., Ishigure, K. and Washio, M. (1988) Pulse-radiolysis study on the yield of hydrated electron at elevated temperatures. J. Phys. Chem. **92**: 3011–3017.
60. Thomas, J. K. and Bensasson, R. V. (1967) Direct observation of regions of high ion and radical concentration in the radiolysis of water and ethanol. J. Chem. Phys. **46**: 4147–4148.
61. Buxton, G. V. (1972) Nanosecond pulse radiolysis of aqueous solutions containing proton and hydroxyl radical scavengers. Proc. R. Soc. Lond. **A 328**: 9.
62. Belloni, J., Billiau, F., Delaire, J. A., Delcourt, M. O. and Marignier, J. L. (1983) Ionizing radiation-liquid interactions: A comparative study of polar liquids. Radiat. Phys. Chem. **21**: 177–183.
63. Draganic, Z. D. and Draganic, I. G. (1975) Formation of primary reducing yields (G_{eaq^-} and G_{H2}) in the radiolysis of aqueous solutions of some positive ions. Int. J. Radiat. Phys. Chem. **7**: 381–386.

Received on September 22, 2005
Revision received on January 24, 2006
Accepted on January 30, 2006